Original Research *Feature article*

Discovery of vascular Rho kinase (ROCK) inhibitory peptides

Reza Abbasgholizadeh[1,2,*], Hua Zhang[1,*], John W Craft Jr[1,2,*], Robert M Bryan Jr[3], Steven J Bark[1], James M Briggs[1], Robert O Fox[1], Anton Agarkov[4], Warren E Zimmer[5], Scott R Gilbertson[4] and Robert J Schwartz[1,2]

[1]Department of Biology and Biochemistry, University of Houston, Houston, TX 77024, USA; [2]Texas Medical Center, Texas Heart Institute, Houston, TX 77024, USA; [3]Department of Anesthesiology, Baylor College of Medicine, Houston, TX 77030, USA; [4]Department of Chemistry, University of Houston, Houston, TX 77024, USA; [5]Department of Medical Physiology, Texas A&M Health Science Center, College Station, TX 77843, USA

Co-corresponding authors: Warren E. Zimmer: WEZimmer@medicine.tamhsc.edu and Robert J Schwartz. Email: rjschwartz@uh.edu

*These authors contributed equally to this paper.

Impact statement

Rho-activated kinases, known as ROCK(s), are significant signaling components in cells that lead alterations in cellular function. The central role of ROCK in smooth muscle cellular homeostasis makes it an important therapeutic target. Small molecule kinase inhibitors target enzyme active site competing for ATP binding. Although effective, ATP binding active sites are similar among very different kinases, and many small molecule inhibitors suffer from non-specific inactivation which as therapeutics can lead to substantial side effects. Here, we designed experiments to identify ROCK inhibitors that do not target ATP binding, rather develop peptides that inhibit ROCK in the presence of ATP. We identified a peptide that binds the activation loop of the enzyme and effectively inhibits activity. This will allow a development of a new class of drugs with exquisite specificity for the ROCK kinases and potentially revolutionize treatment of high blood pressure, cardiac hypertrophy, and many more diseases.

Abstract

Rho-activated kinases (ROCKs) regulate many cellular functions such as proliferation, migration, and smooth muscle contractility, but they are also associated with pathogenesis of many human diseases such as heart failure and hypertension. We used phage display libraries to identify inhibitory polypeptides that bind to the ROCK1 catalytic domain, but do not compete with the ATP-binding pocket, by screening in the presence of high ATP concentrations (1 mM). Peptide7, a promising ROCK inhibitory peptide for both ROCK isoforms, measured at 1.45 ± 0.28 μM for ROCK1 (1–553) and 5.15 ± 1.15 μM for ROCK2. Peptide7 reduced cellular migration in wound healing assays. The binding epitope on ROCK1 was mapped to the flexible activation loop within the catalytic domain. Peptide alanine scanning mutants helped identify critical amino acids to generate optimized Peptide22. This compact ROCK inhibitor facilitated vascular relaxation, blocked neovascularization of endothelial cells, and inhibited MLC phosphatase phosphorylation. Our novel ROCK peptide inhibitors may provide potential treatment of hypertension and PAH progression.

Keywords: Drug design, peptide discovery, Rho kinase inhibitor, phage display, kinase activation loop

***Experimental Biology and Medicine* 2019; 244: 940–951. DOI: 10.1177/1535370219849581**

Introduction

Rho-activated kinases (ROCKs) are a major regulator of physiological processes such as cell adhesion, cell morphology, cell motility, and smooth muscle contraction that are associated with actin cytoskeleton dynamics and generation of actin-myosin contractility.[1–5] This regulation is achieved by phosphorylation of several downstream targets such as myosin light chain (MLC), the myosin binding subunit of myosin phosphatase (MYPT1), LIM kinases, adducin, and the ERM proteins.[2,3,5–7] Both ROCK isoforms are involved in a broad range of human diseases such as cardiovascular disorders,[1,3,8] metabolic and neurologic disorders,[9–11] cancer,[6,8,12] and glaucoma.[13] Attenuation of ROCK signaling effectively reduced progression in many preclinical models of cardiovascular diseases, including agonist- or myocardial infarction-induced pathologic cardiac remodeling, hypertrophy, heart failure,[10,14] high blood

pressure and hypertension,[15] pulmonary arterial hypertension (PAH),[16–19] atherosclerosis,[20] and endothelial dysfunction.[21,22] Thus, ROCK is an important therapeutic target for these diseases and stirs great interest in the development of novel inhibitors of the ROCK signaling pathway.

ROCKs are down-stream effectors of the small GTP-binding protein, RhoA, and have two isoforms, ROCK1 (p160ROCK, ROKb) and ROCK2 (ROKa). ROCK1 and ROCK2 are highly homologous in their kinase catalytic domain (92% and 65% similarities in their kinase domain and overall sequences, respectively).[20,23,24] This serine–threonine kinase is composed of three domains including the N-terminal catalytic domain, a coiled-coil and Rho-binding-binding domain (RBD) and the C-terminal Pleckstrin homology domain (PH domain) that contains an internal cysteine-rich region.[20,23–26] ROCK activity is negatively regulated by the PH domain.[20,23,27–29] Activated Rho-GTP activates ROCK by binding to its RBD, which disrupts the interaction between the C-terminal inhibitory region and the kinase domain, leading to displacement of the PH domain and kinase activation (Figure 1(a)).

Several molecules inhibit ROCK activity[25,30–32] and among the most widely studied are fasudil[33] and Y-27632.[34] Fasudil attenuates cerebral vasospasm caused by subarachnoid hemorrhage.[31,35] Also, Y-27632 is a potent ROCK inhibitor that has been used to study ROCK activity in numerous systems.[25,36] Most of the current small molecular inhibitors of ROCK are type I, which target the ATP-binding pocket of the ROCK catalytic domain in its active conformation, competing with ATP.[23] Both Y-27632 and fasudil bind to ROCK1 and ROCK2 due to 92% identity in their kinase domain sequences and, at higher concentrations, can inhibit other serine–threonine kinases including PKA and PKC.[23,37,38] To avoid selecting compounds that bind to the ATP pocket, we used phage display libraries to identify inhibitory polypeptides that were capable of blocking ROCK1 activity in the presence of high concentrations of ATP (1 mM). This approach led to identification of an inhibitory peptide, Peptide7, and others with similar sequences.

The binding epitope for Peptide7 was mapped to the activation loop on ROCK1 using a chemical cross-linking reagent. Alanine scanning and truncated mutants of

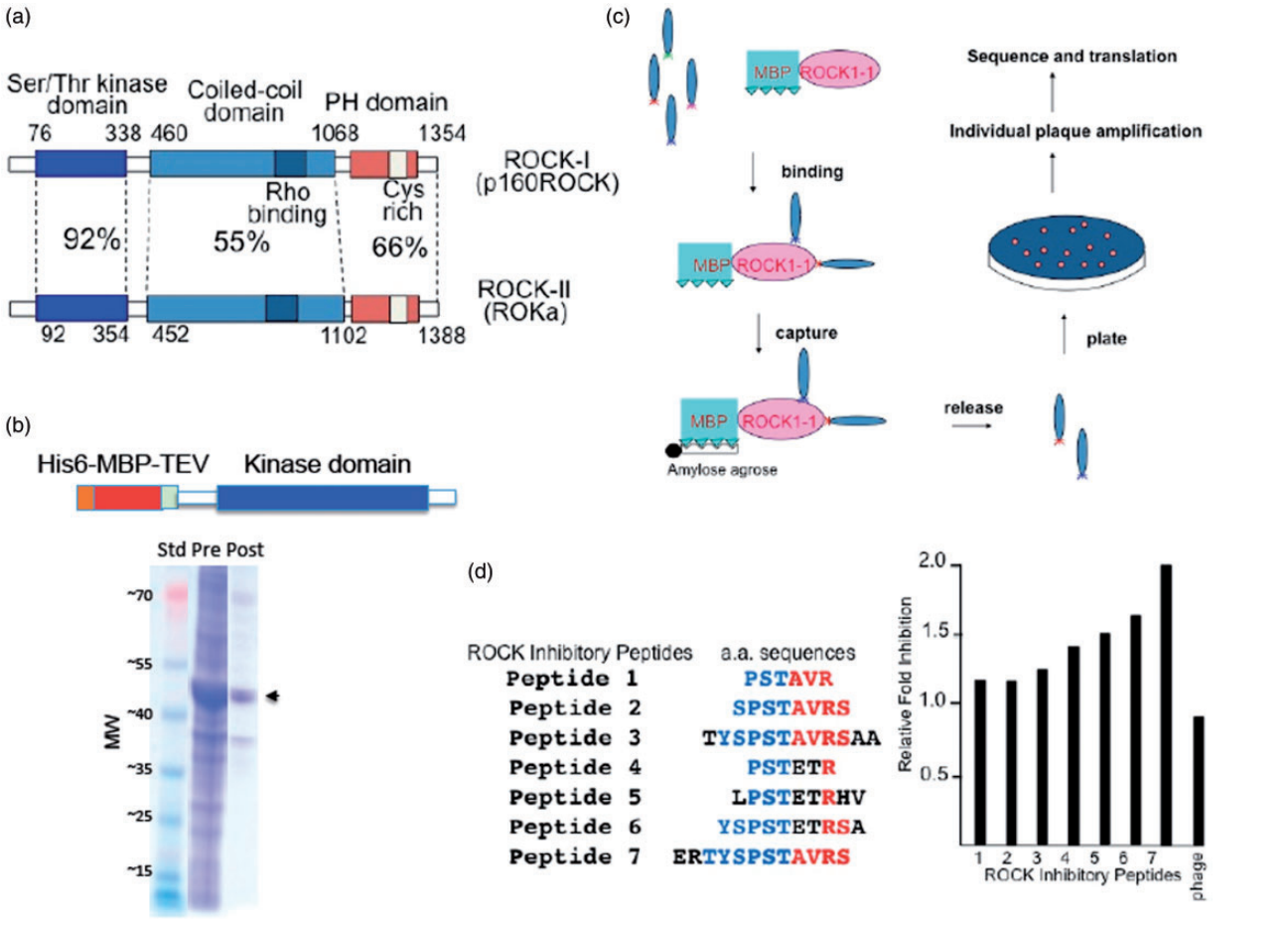

Figure 1. Identification of enriched phage display peptides that inhibit ROCK1 autophosphorylation. (a) Structure of ROCK1 and ROCK2 contains an N-terminal kinase domain (92% identity), followed by a coiled-coiled region containing a Rho-binding domain (RBD), and a C-terminal cysteine-rich domain located within the pleckstrin homology (PH) motif domain. (b) The catalytic domain of ROCK1 (5–348) was fused to the maltose-binding protein (MBP) and expressed in baculovirus expression system, and (c) was incubated with the Ph.D-12 phage display library of 12 amino acids in length under high ATP levels (1 mM) to screen for peptides with strong binding affinity to ROCK N′ terminal catalytic domain. (d) Identification of Rock inhibitory peptides by the luciferase-based kinase assay. Several inhibitory peptides shared overlapping amino acid sequences with the strongest ROCK1 inhibitor, peptide7 (ERTYSPSTAVRS) in the N′ terminal (blue lettering) and the C′ terminal (red lettering) ends. (A color version of this figure is available in the online journal.)

Peptide7 were used to identify amino acids critical for contacting ROCK1's activation loop. Optimized shorter 7 amino acid peptides such as Peptide22 facilitated vascular relaxation, blocked neovascularization (NV) of endothelial cells (ECs), and inhibited MLC phosphatase phosphorylation. We demonstrated that inhibition of the Rho/ROCK pathway may provide potential beneficial treatment in controlling hypertension and PAH progression. The discovery of highly selective and effective Rho kinase inhibitory peptides (Peptide7 and Peptide22) highlights the activation loop of ROCKs, as a novel locus for designing a new class of highly specific inhibitory drugs.

Materials and methods

All animal studies were approved by the Institutional Animal Care and Use Committee (IACUC) of Baylor College of Medicine. Mice used in these studies were back-crossed on C57BL6 background for 10 generations.

Cloning, overexpression, and purification of MBP-ROCK1 (5–348) in E. coli

All recombinant DNA techniques were performed according to published procedures.[39] The ROCK fragments were PCR amplified from plasmid pBSP1603′UTR—full length ROCK1. The sequences of the primers used to amplify ROCK1 were as follows: F: 5′-GGGGACAAGTTTGTACAAAAAA*gaaaacctgta ttttcagggc*GACAGTTTTGAGACTCGATTTG-3′, R: 5′-GGGGACCACTTTGTACAAGAAAGCTGGGTC*tta*GAGCGTTTCCCAAGCCCACT G-3′. Underlined sequences were for Gateway system and Italic sequences indicate TEV cleavage site and stop codon. ROCK1 fragment was intergraded into plasmid PLP16 as His6-MBP-TEV-ROCK1. The construct PLP16-ROCK1 was used to transform the expression host strain *E. coli* BL21 (DE3). For large-scale production of ROCK, 0.5 mM isopropyl-1-thio-β-D-galactopyranoside (IPTG) induction and 16°C overnight expression temperature were used to obtain induced culture. Cells were harvested by centrifugation and disrupted by sonication. For MBP-ROCK1 (5–348) purification, all manipulations were carried out at 4°C. Standard Ni-resin purification procedure was followed as instructed in pET system Invitrogen manual.

Cloning, overexpression, and purification of ROCK2 (20–415) in baculovirus system

All recombinant DNA techniques were performed according to published procedures.[40] Briefly, the DNA fragments containing *ROCK2* gene were amplified by PCR from plasmid pBSP1603′UTR—full length ROCK2. The sequences of the primers used to amplify *ROCK* were as follows: Forward: 5′-CTGCTGCGGGATCCCAAATCG-3′ Reverse: 5′-GAATTCTCGAG*tta*TCTGTTATCATTAGGATTTG-3′. Underlined sequences were inserted as restricted enzyme sites BamHI and XhoI. ROCK2 fragment was integrated into plasmid pFastBac HT-A. Exponentially growing Sf9 cells were infected with recombinant baculovirus at an m. o.i. of 1. After 64 h, Sf9 cells were harvested. ROCK2 was purified using standard Ni-resin purification procedure which was followed according to the Invitrogen pET system manual.

Screening the inhibitory peptides from phage display assay

The procedure was followed according to the New England BioRad phage display protocol. Briefly, 10^9 phage particles were mixed with MBP protein at room temperature for 1 h to avoid the negative selection by eliminating phages that could bind to MBP. After 1 h, the complex of MBP proteins and bound phages were trapped and pulled down using amylase resin. The supernatant which contained only non-MBP-binding phages was incubated with MBP-ROCK1 (5–348) at room temperature for 1 h. The fresh amylase resin was added into the enzyme–phage mixture to pull down the complex of MBP-ROCK and bound phages. The resin was washed nine times using TBS, and the bound phages were eluted from amylase resin using 0.2 M Glycine-HCl. Three rounds of panning procedure were carried out. The stringency was gradually increased at each round by raising the Tween 20 concentration starting at 0.1% to 0.5% in the second round and shortening the binding time from 30 min to 20 min for the second round and 10 min for the third round. *E. coli* HB101 cells were infected with eluted phages and grown. DNAs were extracted and sequenced to determine the sequences of bound peptides.

Luminescent kinase assay

Phage particles from 1 ml of culture was precipitated and dissolved into 50 μL of TBS. Ten microliters of phage containing TBS ($\sim 10^9$ pfu) individually was mixed with 3.5 μM MBP-ROCK1-1 and 10 μM ATP. The consumption of the ATP was monitored by the luminescent assay.

Luciferase-based kinase assay

Quantitative analysis of kinase activity was performed using Kinase-Glo™ kinase assay kit (Promega) according to the manufacture's manual. Briefly, kinase assays were carried out in 384-well white plates in a total volume of 10 μL of 4 ng ROCK1 in kinase buffer (40 mM Tris, 7.5; 20 mM $MgCl_2$; 0.1 mg/ml BSA; 50 μM DTT) in the presence of 0.2 μg/μl S6 peptide (Rho Kinase substrate) and 5 μM ATP and with the inhibitory peptide or DMSO. The reaction was incubated for 1 h at room temperature and then equal volume of Kinase Glo reagent was added to each well, the plate was further incubated for 40 min and luminescence was read in microplate reader. The percent inhibition was calculated relative to an enzyme control without inhibitor. IC50s were calculated by four-parameter nonlinear regression using Prism software (GraphPad Software, La Jolla, CA).

Cross-linking reaction

Inhibitory peptide (Peptide7) was mixed with 30 μg MBP-ROCK at 1:1 ratio in 200 μL of PBS buffer, and the mixture was incubated at room temperature for 20 min. The mixture was loaded into 25 μL prewashed amylase resin for 30 min. Tubes were taped occasionally to ensure better binding.

Resin was washed with 200 μL PBS buffer three times and re-suspended in 200 μL of PBS. Washed resin was mixed with 20 μL of disuccinimidyl suberate (DSS) from 100 μM of stock solution and incubated at room temperature for 15 min and washed with 200 μL of PBS three times again. The resin was analyzed by mass spectroscopy. The control sample was prepared following the same procedure, however, without the presence of the inhibitory peptide.

Surface plasmon resonance

The binding affinity of the inhibitory peptide and ROCK was measured by surface plasmon resonance (SPR) method using Biacore 2000 apparatus. Approximately 440 response units (RU) of MBP-ROCK1 (5–348) and ROCK2 (20–415) were covalently immobilized on the surface of CM5 sensor chip using amine-coupling reaction. The immobilization procedure was followed according to the manufacturer manual. Phosphate buffered saline (8 mm Na_2HPO_4, 1.5 mm KH_2PO_4, pH 7.4, 2.7 mm KCl, 137 mm NaCl, and 0.005% Tween 20) was used as running buffer. The flow rate of 30 μl/min was maintained during SPR measurements.

Saturation transfer difference-NMR

NMR samples were prepared according to the following procedure: 10 μM ROCK (20–415) protein (purified with PBS buffer with no Tris content) were mixed with 0.2 mM inhibitory peptide in 500 μL of PBS buffer containing 5% D_2O. Control samples were 10 μM ROCK alone and 0.2 mM inhibitory peptide alone. The NMR data were collected using saturation transfer difference-NMR (STD-NMR) method, developed by the Keck/IMD NMR Center at the University of Houston.

Detection of apoptosis

To identify apoptotic cells in cultured cells, the terminal deoxynucleotidyl transferase (TdT)-mediated dUTP end labeling (TUNEL) assay was performed using TUNEL Apoptosis Detection Kit from Millipore (CA, USA) according to the manufacturer's instructions.

Cell culture

NIH-3T3 and Hela cells were purchased from ATCC and were grown and maintained in HyClone™ DMEM medium with 10% fetal bovine serum (FBS) and 1% penicillin-streptomycin. Human umbilical vein endothelial cells (HUVEC) were purchased from ThermoFisher Scientific (USA) and were grown and maintained in LSGS-supplemented medium 200PRF containing 2% (v/v) FBS and 3 ng/ml bFGF (ThermoFisher Scientific, USA).

Actin immunofluorescence staining

NIH-3T3 cells (1×10^4/well) were plated onto eight-well chamber slides in serum-free medium with the presence/absence of ROCK inhibitor. After 24 h, cells were washed with PBS twice and fixed with 4% paraformaldehyde in PBS, rinsed in PBS three times, and blocked/permeablized in PBS containing 0.5% Triton X-100 and 5% BSA. Cells were washed and stained with Alexa-Fluor 488-conjugated phalloidin (Invitrogen) to allow visualization of actin filaments. Cells were washed three times with PBS and mounted using Prolong Gold Anti-fade reagent (Life Technologies). The content of F-actin was determined by fluorescence microscopy.

Wound healing assay

Hella cells (2×10^4/well) were plated onto eight-well chamber slides. After 24 h incubation, cells grew to 100% confluence and were wounded with a sterile pipette tip to remove cells by two perpendicular linear scratches. Floating cells were washed off with three times PBS buffer wash before serum-free DMEM medium with the presence or the absence of ROCK inhibitor was added into wells. Cells were incubated in a 5% CO_2 incubator at 37°C. The cell migration in each group was observed and photographed at 0 h and after 12 h and 24 h. The gap distance was measured for each cross using the NIS-Elements AR software by Nikon and changes in migration were calculated using the following formula: Change in migration (%) = [distance (0 h)–distance (24 h)]/distance (0 h) ×100% and reported as mean ± SD for at least three independent experiments.

Isometric tension from aortic ring

Changes in isometric force were measured as described previously.[41,42] Briefly, young adult (eight weeks) mice pairs were deeply anesthetized with a ketamine-xylazine-acepromazine combination followed by administration of 50 units of heparin. Under sterile conditions, the abdominal aorta was opened, and the thoracic aorta was flushed with ice-cold HBSS via cardiopuncture. The thoracic aorta was carefully removed, placed into a dish containing ice-cold HBSS, and cleaned of connective tissue and visceral fat. The aortae were cut into 2-mm rings from the proximal end and mounted on metal stirrups attached to a myography (ChuelTech, Houston, TX). Each aortic ring was suspended in a water-jacketed organ bath (22 ml) maintained at 37°C. The rings were allowed to equilibrate for 60 min under minimal force followed by slowly increasing the force to a resting tension of 1.2 mN, which was maintained throughout the experiment. Rings were then contracted with 40 mmol/l KCl in Krebs buffer (in mmol/l): 119 NaCl, 4.7 KCl, 1 $MgSO_4$, 1.2 KH_2PO_4, 24 $NaHCO_3$, 11 glucose, 2.5 $CaCl_2$, and washed with normal Krebs buffer (KCl 5.4 mmol/l) after full contraction were observed. Rings were repeatedly contracted with 40 mmol/l KCl in Krebs buffer until the force developed was constant from 2-consecutive contractions. Only one experiment was performed on each aortic ring. At the end of each experiment, rings were contracted with 40 mmol/l KCl to ensure the healthiness of the rings and validate the acquired results. Isometric force was measured at 37°C in Krebs buffer. The buffer was equilibrated with a gas consisting of CO_2 5%/O_2 20%/N_2 balance for pH = 7.4. Krebs buffer was refreshed every 20 min. Changes in force in each ring were measured using a Research Isometric Transducer (Harvard Apparatus, Holliston, MA). Ring contraction data were acquired and analyzed using

Powerlab/8sp (AD Instruments, Colorado Springs, CO) at 10 Hz by LabChart v4.2.4 (AD Instruments).

Tube formation assay

HUVECs ($1.8–2.2 \times 10^4$ cells/well) in LSGS-supplemented medium 200PRF containing 2% (v/v) FBS and 3 ng/ml bFGF (ThermoFisher Scientific, USA) with the presence/absence of Rho-Kinase inhibitor were seeded in 48-well plates precoated with 100 μL of Geltrex (ThermoFisher Scientific, USA). Cells were incubated at 37°C, 5% CO_2. Images were taken 12 h post-seeding by Nikon light microscope. For quantification of tube networks, Image J with the Angiogenesis Analyzer plugin was used analyze the images and the average mesh sizes in treated/non-treated cells were calculated as mean ± SD for at least three independent experiments. Cells used for every experiment using this assay had passage numbers less than four.

Immunoblot analysis

HUVECs were passaged onto six-well plates and treated with/without ROCK inhibitor in serum-free medium. Twenty four hours post treatment, cells were washed two times with ice cold PBS buffer and were lysed in ice cold RIPA buffer with protease and phosphatase inhibitor tablets (Roche, Basal, Switzerland). Cells were then incubated on ice for 15 min and spun at 14,000 r/min for 5 min. Lysates were stored at −80°C until further use. A bicinchoninic acid assay (Life Technologies) was performed to determine the protein concentration. Thirty micrograms of proteins were loaded and run on a 4–12% Bis-Tris Plus Gel (Life Science, USA), followed by a transfer to a nitrocellulose membrane. The membrane was blocked for 1 h at 25°C in Tris-Buffered Saline plus Tween-20 solution (TBST). The membrane was incubated with 1:1000 dilution of anti-MYPT1, anti-phospho-MYPT1 T853, or GAPDH (Cell Signaling Technology In., Danvers, MA) primary antibodies in TBST buffer overnight at 4°C. The membrane was washed three times in TBST and then probed with a 1:5000 dilution of corresponding HRP-conjugated secondary antibody (Cell Signaling Technology). Signals were visualized using SuperSignal™ West Femto Maximum Sensitivity Substrate kit from ThermoFisher Scientific. Quantification analysis was performed using Image J (Ver. 1.46). GAPDH quantification was used to account for differences in protein loading, and the signals obtained for each protein were normalized to GAPDH and plotted as mean ± SEM for at least three independent experiments.

Results

Identification of a Rho kinase inhibitory peptides by screening phage display libraries

The major challenge for developing a protein kinase inhibitor is to specifically target that particular protein kinase. One of the rational ways to achieve this goal is to find or design an antagonist that can target the regulatory domains of the kinase instead of the highly conserved ATP-binding pocket. Phage display is a powerful research tool for high-throughput screening of protein interactions.[43,44] The catalytic domain of ROCK1 (5–348) (Figure 1(a)) fused to the maltose binding protein (MBP) (Figure 1(b)) allowed for serial enrichment of phage by repeated passages through amylose agarose (Figure 1(c)). We conducted the screening procedure under high levels of ATP (1 mM) to detect peptides that bind to the ROCK N′ terminal catalytic domain of ROCK. Peptides with consensus sequences, R/K-X-S/T or R/K-X-X-S/T present in ROCK substrates were culled from our candidate list. Next, sequencing of a focused group revealed several peptides that shared overlapping sequences shown in Figure 1(d), such as YSPST (blue) and or ASVRS (red), which culminated in the strongest ROCK1 inhibitor, peptide7 (ERTYSPSTAVRS).

Peptide7 binds to activation loop of Rho kinase

Cross-linking reactions between ROCK1 catalytic domain and Peptide7 were performed to determine the Peptide7 binding site. (Figure 2(a)). Among the tryptic peptides analyzed by MALDI-TOF-MS, we observed a unique peptide with m/z of 1430.1 only present from DFDNB cross-linked inhibitory Peptide7/ROCK kinase complex. This peptide was absent in the tryptic peptide in samples cross-linked with only ROCK (Figure 2(b)). The unique peptide corresponded to Peptide7 (ERTYSPSTAVRS) binding to MNKEGMVR fragment on ROCK, which is located on the edge of ROCK's activation loop (Figure 2(c)). Interestingly, the "Activation Loop," which in many kinases is the site of regulatory phosphorylation or interaction with activity modulators,[24,38] showed considerable structural diversity. This diversity extended from the C-terminal portion of β9 strand to the αEF coil. The most exciting aspect of identifying the activation loop, as a site for targeting drugs, is their virtual specificity for each kinase; thus, increasing the chances for generating specific protein kinase inhibitors, with little or no cross-inhibitory activity.

The strength of interactions between Peptide7 and ROCK1 and ROCK2 was then analyzed by performing an SPR study (Supplemental Figure 1). The binding of Peptide7 to ROCK1 as compared to ROCK2 demonstrated small differences even though bith proteins have 92% similarity in sequence in the catalytic domain. Upon inspection, there are only 3 amino acid differences in the activation loop (Supplemental Figure 2). The average of three experiments yielded K_D values of 1.458 ± 0.28 μM for ROCK1 (1–553) and 5.153 ± 1.15 μM for ROCK2. Interestingly, slight differences in the K_D values of ROCK1 and ROCK2 are consistent with findings from cross-linking and STD-NMR studies (Supplemental Figure 3), suggesting the Activation Loop of ROCK, as the Peptide7 binding site.

Peptide7 disrupted the cellular cytoskeleton and reduced cell migration

The biological activity of Peptide7 was investigated by studying the changes of cytoskeletal actin filaments and by a wound healing assay, shown in supplemental data. To facilitate cellular intake and permeability, Peptide7 was synthesized with addition of TAT sequence at its N′

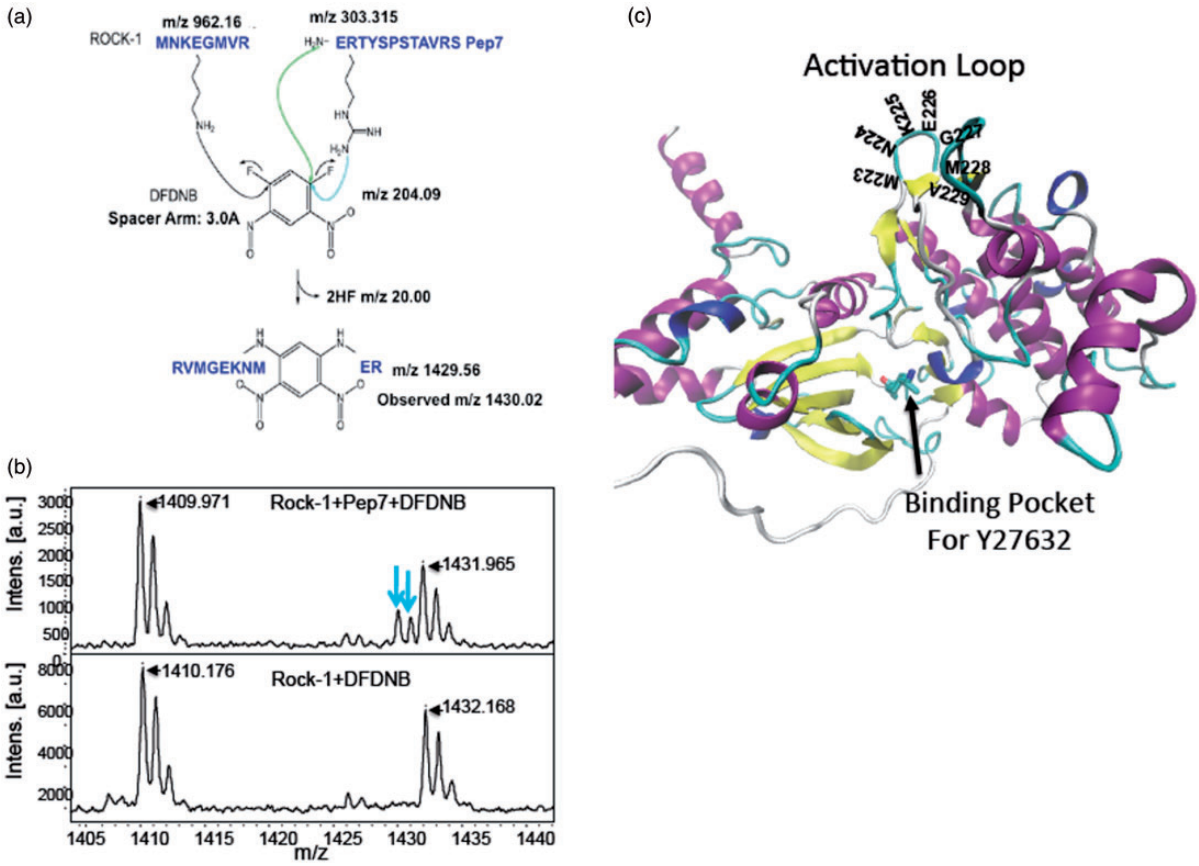

Figure 2. Mapping Peptide7 binding epitope in ROCK1 using crosslinking, trypsin digestion, and mass spectroscopy. (a) Highly purified MBP-ROCK1 was mixed with Peptide7 and cross-linking reagent DFDNB. MBP-ROCK1 plus cross-linked Peptide7 were digested with Trypsin and (b) the peptide fragments were detected by mass spectroscopy, as described in Materials and Methods section. The top panel is from Peptide7 and ROCK complex cross-linking reaction. The bottom panel is ROCK alone cross-linking reaction. Arrows point at the peak m/z 1430.02. The peaks represent the DNFB linking Peptide7 and ROCK-1 segment corresponded to Peptide7 binding to the fragment MNKEGMVR on the active loop of ROCK1. (c) X-ray crystal structure of the ROCK1 catalytic domain showed the activation loop that overlaps with the fragment sequence. (A color version of this figure is available in the online journal.)

end terminal (TAT-peptide7). The HIV Tat-derived peptide (RKKRRQRRR) is a small basic peptide that has been successfully shown to deliver a large variety of cargo, from small particles to proteins, peptides, and nucleic acids.[25] No significant change in the number of apoptotic cells (FITC-positive) was observed in TAT-peptide7-treated NIH-3T3 cells and HUVECs up to 200 μM, indicating the safe dose of TAT-peptide7 at 200 μM (data not shown). The effect of TAT-peptide7 on actin-cytoskeleton was assessed in HUVECs (Supplemental Figure 4(a)). Actin stained cells treated with 100 μM TAT-peptide7 for 24 h exhibited disassociated or "melted" cellular actin cytoskeleton, similar to ROCK inhibitor, Y-27632. The TAT polypeptide sequence alone was ineffective. By dynamically regulating the cytoskeleton, ROCK plays an important role in cell attachment, migration, and contraction events that are critical to wound healing.[45] Also, TAT-peptide7 efficiently reduced wound healing by almost 29% compared with the non-treated cells, and this inhibition was not mediated by TAT peptide (Supplemental Figure 4(b)).

Identification of essential residues of Peptide7

To identify the critical amino acid residues of Peptide7 that determines its inhibitory property, we synthesized alanine-substituted mutants, so that a single alanine was substituted for each original amino acid in Peptide7, as shown for Peptides 8 through 18 (Figure 3(a)). Alanine substitutions for glutamic acid, tyrosine, serine, and proline drastically reduced the inhibitory efficacy of the peptide, indicating the importance of the YSPS residue in the inhibitory function of the peptide (Figure 3(a) and (b)). STD-NMR was used to observe the resonances from peptide atoms that are in contact with ROCK. The STD spectrum demonstrated that an interaction exists between ROCK and Peptide7 by displaying resonances at 6.8 and 7.0 ppm from Peptide7 Tyr Hε and Hδ and 2.85–2.9 ppm from Tyr Hβ (Supplemental Figure 3). These results indicate that Peptide7 (ERTYSPSTAVRS) makes contacts with ROCK that include the unique Tyr residue. TOCSY and ROESY NMR experiments on the free peptide were also collected and assigned using backbone ROE transfer information. Interestingly, the signal from tyrosine4 on the peptide remained unattenuated, indicative of its role in the peptide-binding interface.

Evaluation of biological activities of Peptide7 and its derivatives. Due to its relatively long sequence of TAT-Peptide7, we chose to optimize for shorter inhibitory

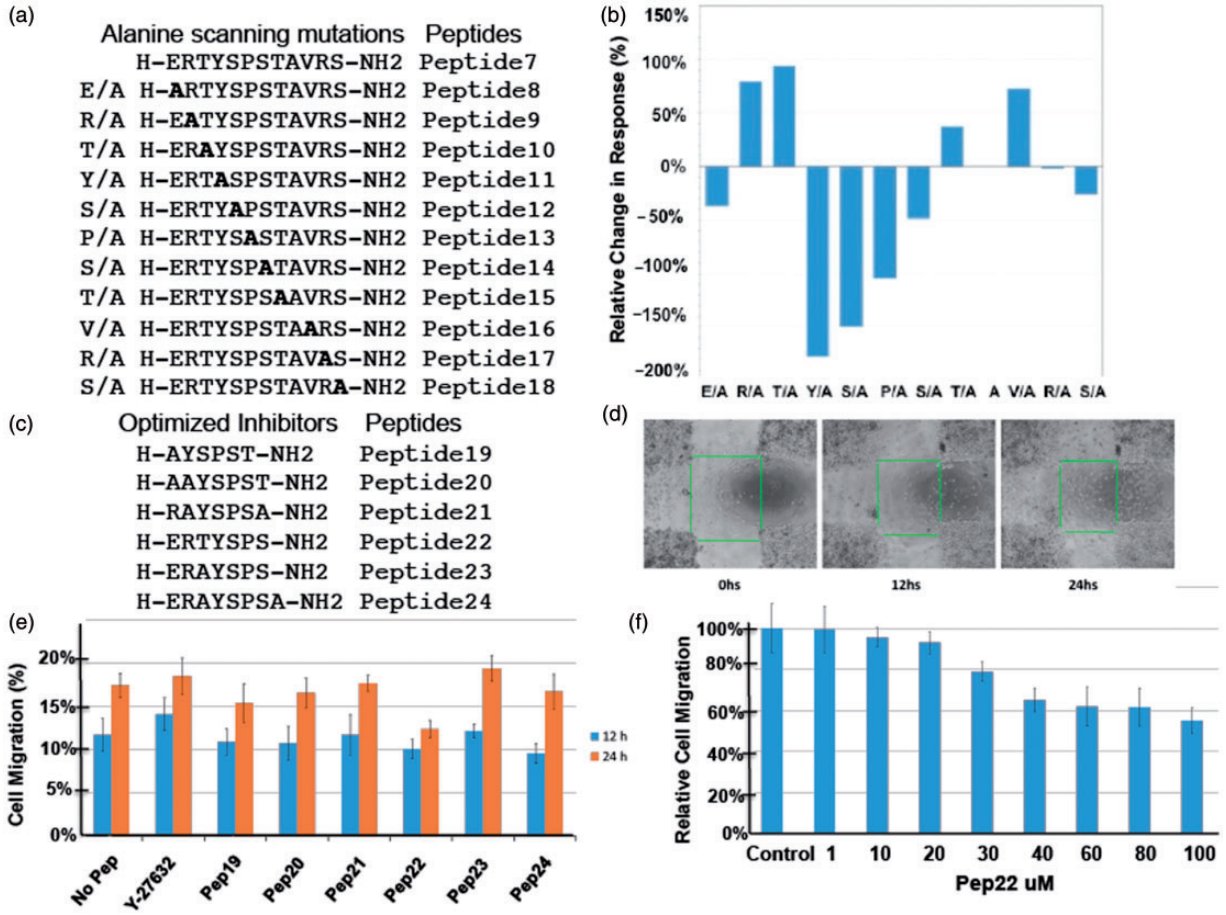

Figure 3. Identification of critical residues of ROCK1 inhibitory Peptide7. (a) Alanine scanning mutations were generated by synthesizing peptides in which an alanine (A) was inserted sequentially from the N′ terminus of Peptide7 to produce Peptides8-18. (b) Peptides were assayed for inhibiting ROCK1 activity by the luciferase kinase assay. Alanine substitution at positions E1, Y4, S5, P6, and S7 all reduced the effectiveness of Peptide7, while the addition of alanine at R2, T3, T8 and V10 enhanced inhibitory activity. (c) Peptides were designed based on Peptide7's critical residues to identify any peptides with enhanced ROCK inhibition. (d) Wound healing assay with cultured Hela cells were treated with 100 μM of Peptides19–24 in serum-free medium in the presence of 0.1% DMSO. (e) Relative cell migration assays (n = 5 trials) revealed Peptide22, as the best inhibitor at dual time points (12 h and 24 h). (f) A dose curve displayed an apparent migratory inhibition between 30 μm and 40 μm of Peptide22. (A color version of this figure is available in the online journal.)

peptide fragments based Peptide7's critical residues. As shown in Figure 3(e), Pep22 (ERTYSPS) inhibited cell migration effectively at 12 and 24 h of treatment. The effective dose of Peptide22 was evaluated by wound healing assay (Figure 3(f)) in which 40 μM, appeared as an optimal biological dose. Next, the phosphorylated/non-phosphorylated ratio of S6, a ROCK substrate, was evaluated in the presence of Peptide22 by mass spectroscopy (Supplemental Figure 5). Peaks representing phosphorylated and non-phosphorylated S6 substrates were quantified led to the observation that Peptide22 repressed the phosphorylation of substrate S6 by ROCK. Bioluminescence-based kinase assay was performed to measure the inhibitory effect of Peptide7 and Peptide22 on the activity of ROCK1. The V_{max} and K_m measurements for ROCK1 kinase activity in the presence or absence of Peptide7 and Peptide22 under 1 mM ATP concentration are summarized in Supplemental Figure 5. In the presence of Peptide22, V_{max} and K_m values showed a significant decrease by approximately 93.9% and 81.0%, respectively, indicating Peptide22's efficiency in inhibiting ROCK activity. In addition, the calculated IC_{50} value of Peptide22 for ROCK1 was 44.4 μM.

ROCK inhibitory Peptide22 caused vascular relaxation. Wire myography was performed to assess the efficacy of our developed ROCK inhibitors on precontracted aorta rings relaxation. It has been reported that stimulation of the TXA_2 receptor can activate downstream Rho-kinase signaling pathway.[27] We used U46619, a TxA_2 (thromboxane A_2) mimetic, which can induce vascular muscle contraction through activation of the Rho-kinase signaling pathways by mediating phosphorylation of MYPT1. To find the effective contractile inducing dose of U46619, following the relaxation of the rings after the KCl contraction, the rings were subjected to contractile assays, by adding different doses of U46619, and 1–3 nM U46619 was chosen as the preferred dose (Supplemental Figure 6). In this regard, the experimental procedure was modified, and rings were pretreated with Peptide22 for 20 min, before induction of contraction (Figure 4, top panel). Next, aortic rings were contracted, by adding the U46619 compound to measure the contraction

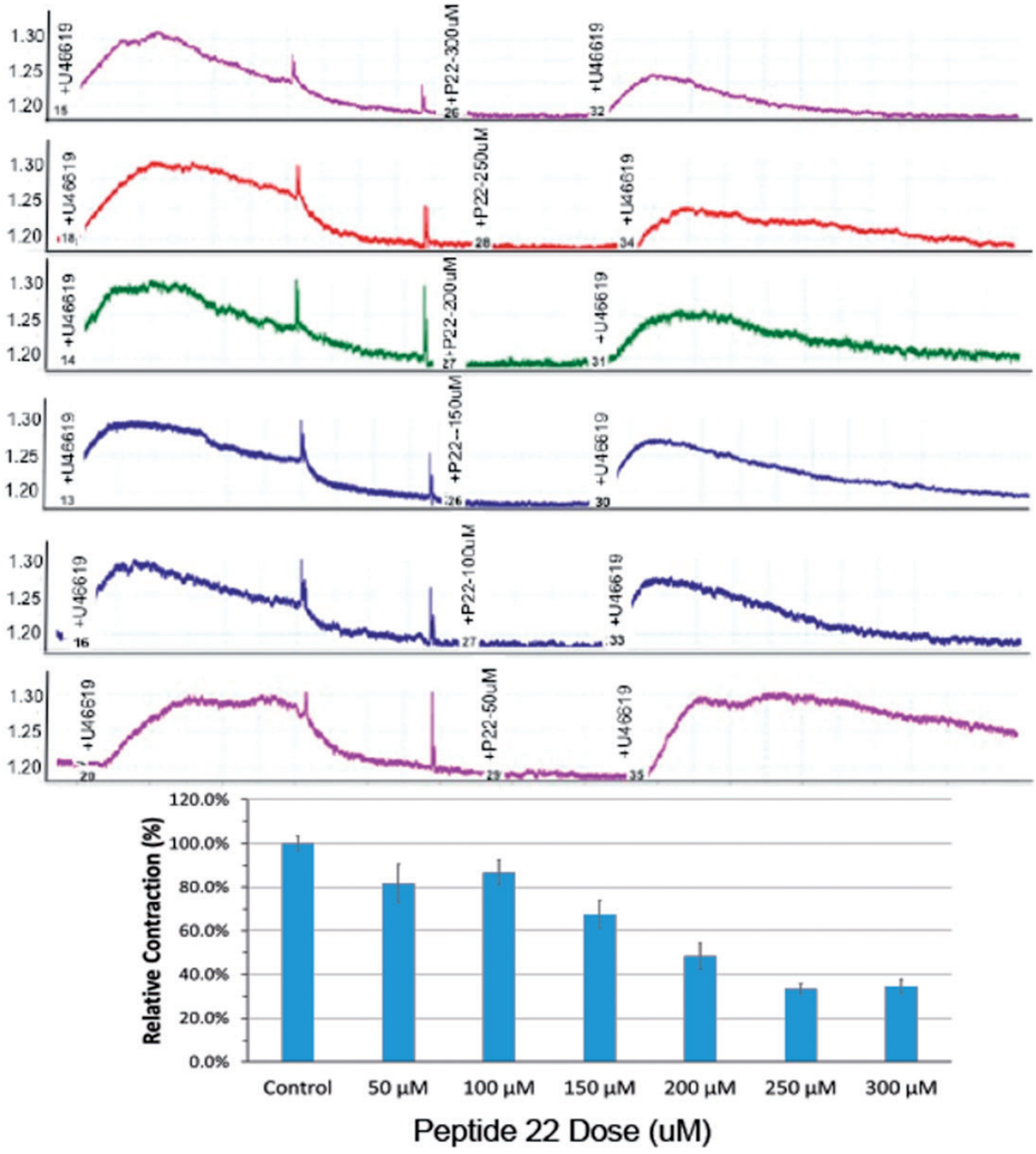

Figure 4. ROCK inhibitory Peptide22 facilitates vascular relaxation. Murine aortic rings were first allowed to contract by adding an optimized dose of the U46619 compound (see Supplemental Figure 6) to identify the contraction force in the absence of peptide22. Next rings were washed with Krebs buffer, were then preincubated with an increasing dose curve of peptide22 (50 µM, 100 µM, 150 µM, 200 µM, 250 µM, and 300 µM) in the presence of 0.1% DMSO for 20 min and then allowed to contract with U46619 (top panel). Incubating aortic rings with different concentrations of the peptide22 showed suppression of U46619 induced contractility in a dose-dependent manner (bottom panel). (A color version of this figure is available in the online journal.)

force in the absence of Pep22. Following the completion of isometric contraction, rings were refreshed twice with Krebs buffer to eliminate U46619 and induce relaxation. Subsequently, rings were pre-incubated with a dose curve from 50 µM to 300 µM) in 0.1% DMSO for 20 min, and then U46619 was applied again to contract the rings. The affect was measured by the difference of the highest response of U46619 in the presence and absence of Peptide22. Experimental results indicated that the Peptide22 showed attenuation of U46619's induced contractility in a dose-dependent manner (Figure 4, bottom panel), thus demonstrating the effectiveness of Peptide22 up to 250 µM with the calculated IC_{50} of 150 µM.

Peptide7 and its derivative Peptide22 inhibit NV. To examine the ability of Peptide7 and its derivative Peptide22 to diminish NV, a tube formation assay was performed in the presence/absence of the inhibitory peptides

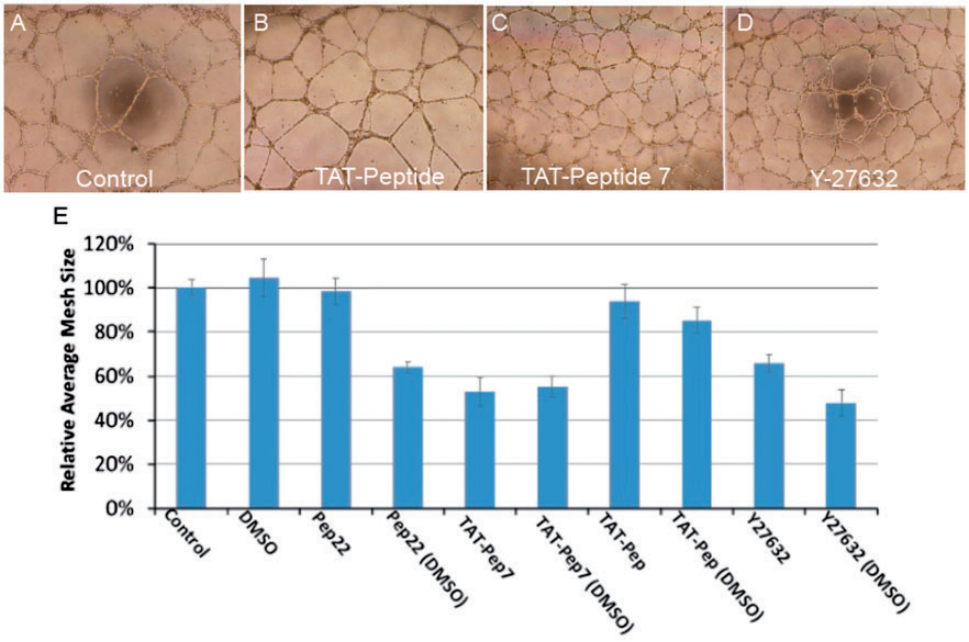

Figure 5. Rock1 inhibitory peptides block neovascularization of endothelial cells. Tube formation assay was performed in the presence and or absence of the inhibitory peptides. HUVECs were incubated with 100 of μM TAT-peptide, 100 μM of TAT peptide7, 100 μM of Peptide22, and 10 μM of Y-27632 in the presence or the absence of 0.1% DMSO for 12 h before image acquisition. Relative average mesh sizes in newly formed tubes were calculated and graphed (n = 3). (A color version of this figure is available in the online journal.)

(Figure 5). HUVECs were incubated with 100 μM of TAT-peptide7, 100 μM of TAT peptide, 100 μM of Peptide22, and 10 μM of Y-27632 in the presence or the absence of 0.1% DMSO for 12 h before image acquisition. Tube formation results (Figure 5(e)) indicate that TAT-peptide7 efficiently reduced the average mesh size to 53.0 ± 6.6% and 55.1 ± 4.9% in the absence and the presence of 0.1% DMSO compared with non-treated cells, and this effect was not mediated by TAT peptide. The efficiency of the observed inhibition was similar to the treatment with 10 μM of Y-27632 in the presence of 0.1% DMSO, which resulted in 47.8 ± 6.2% reduction. Treatment with 100 μM Peptide22 without the presence of 0.1% DMSO did not exhibit any significant inhibitory effect (98.4 ± 6.2%), while the addition of 0.1% DMSO dramatically improved the inhibition efficacy to 64.0 ± 2.3%.

In order to investigate the involvement of Rho kinase pathway and its inhibition in the observed reduction in average mesh sizes, Rho kinase activity was measured as previously described.[46] ROCKs can activate MLC by increasing its phosphorylation directly or through deactivating MLC phosphatase (MYPT1) by phosphorylating and inhibiting its myosin-binding subunit (MBS) (Figure 6(a)).[47] HUVECs were incubated with 100 μM of TAT-peptide7, 100 μM of TAT peptide, 100 μM of Peptide22 and 10 μM of Y-27632 in the presence or the absence of 0.1% DMSO for 12 h. Consistent with the results of tube formation assay, the amount of MYPT1 phosphorylation for each treatment directly correlates with the reduction in relative average mesh sizes, indicating the involvement of Rho kinase in the formation of tubes (Figure 6(b)). TAT-peptide7 attenuated MYPT1 phosphorylation to about 20.0 ± 3.1% and 17.1 ± 5.3% in the absence and the presence of 0.1% DMSO compared with control cells. Predictably, Peptide22 demonstrated robust Rho kinase inhibitory effect, only in the presence of 0.1% DMSO. The percentage of MYPT1 phosphorylation following 12 h treatment with 100 μM of Peptide22 was 60.1 ± 8.7% and 18.4 ± 6.2% in the absence and the presence of 0.1% DMSO, respectively. As for 10 μM of Y-27632 treatment, the amount of MYPT1 phosphorylation was dropped to 30.1 ± 6.1% in the absence of 0.1% DMSO and 14.2 ± 3.0% in the presence of 0.1% DMSO, which is directly proportional to observed attenuation in average mesh size of formed tubes.

Discussion

Rho/Rho kinase pathway is the major regulator of cytoskeletal dynamics and actin-myosin contraction. Its pathophysiologic activity has been linked to progression of many human diseases, which suggests ROCK as a promising target for limiting the pathogenesis of these diseases. Here, we reported the discovery of a highly selective allosteric ROCK inhibitory peptide (Peptide7) that effectively blocked ROCK activity in cell/non-cell-based assays. However, due to its relatively long sequence, Peptide7 contains many cleaving sites and can become a substrate for many endogenous proteases, which can limit and shorten its duration of action. Therefore, we designed several shorter peptides based on the identified critical residues of Peptide7 and evaluated their ROCK inhibition efficacy using wound healing assay. Peptide22 (ERTYSPS) was identified as the most efficient peptide among other peptides, inhibited ROCK more effectively in a dose-dependent manner with 40 μM identified as the minimum dose of Peptide22 showing the maximum response (Figure 2).

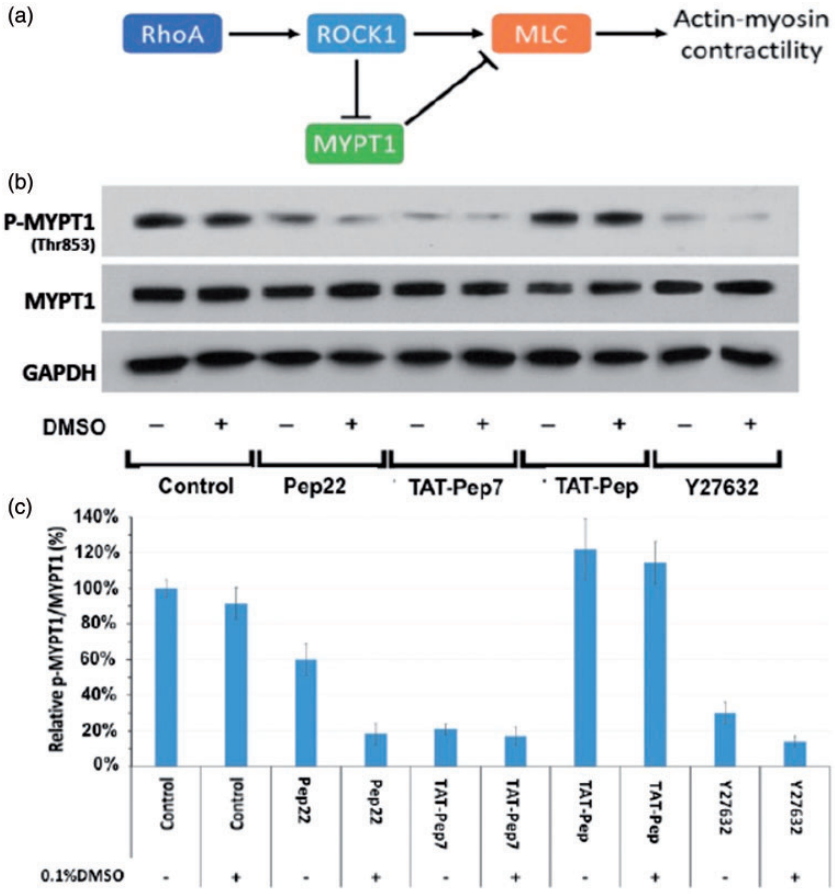

Figure 6. Rho kinase pathway peptide inhibitors inhibited MLC phosphatase phosphorylation. (a) ROCKs can activate myosin light chain (MLC) by increasing its phosphorylation directly or through deactivating MLC phosphatase (MYPT1) by phosphorylating and inhibiting its myosin-binding subunit (MBS). (b) HUVECs were incubated with 100 μM of TAT-peptide7, 100 μM of TAT peptide, 100 μM of Peptide22, and 10 μM of Y-27632 in the presence or absence of 0.1% DMSO for 12 h. The amount of MYPT1 phosphorylation for each treatment was measured through immunoblotting (n = 3). (A color version of this figure is available in the online journal.)

Increased myocardial fibrosis is one of the major causes of heart failure due to increased myocardial stiffness and eventual systolic dysfunction.[48,49] Myocardial stiffening is mainly caused by excess production and accumulation of collagen, one of the extracellular matrix structural proteins which might be due to hyperactivity of existing fibroblasts or migration and recruitment of fibroblast precursor cells that reach myocardium and transform into fibroblasts.[50] ROCK contributes to the pathogenesis of fibrosis through different mechanisms including promoting migration of myofibroblasts to the site of injury in response to released chemokines[50,51] and upregulation of subset of profibrotic cytokines, TGFβ1, TNF-α, and IL-1β,[4,5,52] and its inhibition has shown to attenuate fibrosis progression. As a major regulator of cytoskeleton, ROCK can promote accumulation and stabilization of actin filaments by blocking cofilin-dependent actin depolymerization[53] and thus regulating cell migration.[54] Treating NIH-3T3 cells with TAT-Peptide7 resulted in the disruption of cytoskeletal actin filaments and intense reduction in these cells' migration capability (Supplemental Figure 4).

In addition, the ROCK inhibitory peptide, Peptide22, effectively relaxed the aortic rings contracted through the activation of Rho/ROCK pathway in wire myography. The RhoA/Rho kinase pathway is a major regulator of smooth muscle contraction and its abnormal activity is associated to many vasculature disorders including high blood pressure and PAH. Many vasoactive substances including angiotensin II and serotonin can activate this pathway and promote the pathogenesis of PAH.[10,55,56] In the wire myography assay, preincubating aortic rings with Peptide22, effectively lowered the ring's contractile response to the similar dose of contraction inducer, U46619, and this effect is mediated in a dose-dependent manner with maximum inhibitory effect observed at 250 μM (Figure 4).

Both ROCK inhibitory peptides, Peptide7 and Peptide22, were also shown to be effective in corneal NV model. Formation of new blood vessels, inflammation, edema, and scaring are all characteristics of corneal NV which can compromise visual acuity.[57] Rho/Rho kinase pathway can exacerbate the pathogenesis of the disorder by regulating processes that are involved in NV including EC polarity, cell adhesion, and cell motility.[24,58] Treating HUVECs with 10 μM of Y-27632, 100 μM of TAT-peptide7, and 100 μM of Peptide22 resulted in significant reduced average mesh sizes as compared with control and TAT peptide treated cell (Figure 5). Inhibition of ROCK activity results in reduction in cells ability to migrate, which subsequently translates into formation of narrower tubes. TAT-

peptide7 efficiently reduced the relative average mesh size to 53.0 ± 6.6% and 55.1 ± 4.9% in the absence and the presence of 0.1% DMSO compared with non-treated cells, which is comparable to the activity of widely used ROCK inhibitor, Y-27632 with 65.6 ± 4.1% and 47.8 ± 6.2% reduction in relative average mesh sizes in the absence and the presence of 0.1% DMSO, respectively. Peptide22 was shown to require the assistance of penetration enhancer, DMSO, for its intracellular delivery. There are many reports indicating improvements in drug permeability across biological membranes after the addition of DMSO to the formulation.[38,39] In the presence of 0.1% DMSO, Peptide22 were able to effectively reduce relative average mesh size (64.0 ± 2.3%), while it was shown to be ineffective in the absence of DMSO (98.4 ± 6.2%).

Furthermore, a direct correlation was observed between the decrease in ROCK activity and the reduction in the relative average mesh size of formed tubes during the tube formation assay (Figure 6). ROCK activity was evaluated by measuring the amount of MLC phosphatase (MYPT1) phosphorylation as previously described.[46] TAT-peptide7 attenuated MYPT1 phosphorylation to about 20.0 ± 3.1% and 17.1 ± 5.3% in the absence and the presence of 0.1% DMSO compared with control cells which directly correlates with observed reduction in the relative average mesh size to 53.0 ± 6.6% and 55.1 ± 4.9%, following its treatment in the absence and the presence of 0.1% DMSO. Similarly, ROCK activity remained relatively high (60.1 ± 8.7%) following treatment with Peptide22 in the absence of 0.1% DMSO which resulted in insignificant reduction in relative average mesh size, while it was greatly reduced to 18.4 ± 6.2% in the presence of 0.1% DMSO which let to prominent reduction in relative average mesh size.

Altogether, the results of experiments using these tissue- and organ bath-based models of human diseases indicate the efficacy of both Peptide7 and Peptide22 in controlling the pathogenesis of these diseases at the cellular/organ level and nominate them as promising candidates for further studies. However, more investigation is required to evaluate their activity and efficacy as well as safety in *in vivo* models. This can be achieved by modifying their structure and developing formulation to improve their stability, safety, physiochemical properties, and target delivery which allow them to be applied and evaluated in animal models of human diseases.

Authors' contributions: All authors contributed to the writing and editing of the article. RA, HZ, JWC, contributed equally to the conduct of experiments. RA, HZ, JWC, JMB, ROF, AA, SRG, and RJS contributed to the design of the study with all authors contributed to the analysis and interpretation of the article.

DECLARATION OF CONFLICTING INTEREST

The author(s) declare no potential conflicts of interest with respect to the research, authorship, and publishing of this article.

FUNDING

The author(s) disclosed receipt of the following financial support for the research, authorship, and/or publication of this article: This research was supported by grant to RJS from the Norman Hackerman Fund ARP NH ARP 003652–0231-2009.

REFERENCES

1. Rikitake Y, Oyama N, Wang CY, Wang CY, Noma K, Satoh M, Kim HH, Liao JK. Decreased perivascular fibrosis but not cardiac hypertrophy in ROCK1+/- haploinsufficient mice. *Circulation* 2005;**112**:2959–65
2. Shi J, Zhang YW, Summers LJ, Dorn GW 2nd, Wei L. Disruption of ROCK1 gene attenuates cardiac dilation and improves contractile function in pathological cardiac hypertrophy. *J Mol Cell Cardiol* 2008;**44**:551–60
3. Shi J, Zhang YW, Yang Y, Zhang L, Wei L. ROCK1 plays an essential role in the transition from cardiac hypertrophy to failure in mice. *J Mol Cell Cardiol* 2010;**49**:819–28
4. Zhang YM, Bo J, Taffet GE, Chang J, Shi J, Reddy AK, Michael LH, Schneider MD, Entman ML, Schwartz RJ, Wei L. Targeted deletion of ROCK1 protects the heart against pressure overload by inhibiting reactive fibrosis. *Faseb J* 2006;**20**:916–25
5. Yang X, Li Q, Lin X, Ma Y, Yue X, Tao Z, Wang F, McKeehan WL, Wei L, Schwartz RJ, Chang J. Mechanism of fibrotic cardiomyopathy in mice expressing truncated Rho-associated coiled-coil protein kinase 1. *Faseb J* 2012;**26**:2105–16
6. Georgouli M, Herraiz C, Crosas-Molist E, Fanshawe B, Maiques O, Perdrix A, Pandya P, Rodriguez-Hernandez I, Ilieva KM, Cantelli G, Karagiannis P, Mele S, Lam H, Josephs DH, Matias-Guiu X, Marti RM, Nestle FO, Orgaz JL, Malanchi I, Fruhwirth GO, Karagiannis SN, Sanz-Moreno V. Regional activation of myosin II in cancer cells drives tumor progression via a secretory cross-talk with the immune microenvironment. *Cell* 2019;**176**:757–74 e723
7. Shi J, Wei L. Rho kinases in cardiovascular physiology and pathophysiology: the effect of fasudil. *J Cardiovasc Pharmacol* 2013;**62**:341–54
8. Liu J, Wada Y, Katsura M, Tozawa H, Erwin N, Kapron CM, Bao G, Liu J. Rho-associated coiled-coil kinase (ROCK) in molecular regulation of angiogenesis. *Theranostics* 2018;**8**:6053–69
9. Harbom LJ, Rudisill TL, Michel N, Litwa K, Abeenhakker MP, McConnell MJ. The effect of rho kinase inhibition on morphological and electrophysiological maturity in iPSC-derived neurons. *Cell Tissue Res* 2019;**375**:641–4
10. Liu Y, Suzuki YJ, Day RM, Fanburg BL. Rho kinase-induced nuclear translocation of ERK1/ERK2 in smooth muscle cell mitogenesis caused by serotonin. *Circ Res* 2004;**95**:579–86
11. Wen JY, Gao SS, Chen FL, Chen S, Wang M, Chen ZW. Role of CSE-produced H2S on cerebrovascular relaxation via RhoA-ROCK inhibition and cerebral ischemia-reperfusion injury in mice. *ACS Chem Neurosci* 2018;**10**:1565–74
12. Yuan J, Chen L, Xiao J, Qi XK, Zhang J, Li X, Wang Z, Lian YF, Xiang T, Zhang Y, Chen MY, Bei JX, Zeng YX, Feng L. SHROOM2 inhibits tumor metastasis through RhoA-ROCK pathway-dependent and -independent mechanisms in nasopharyngeal carcinoma. *Cell Death Dis* 2019;**10**:58
13. Pitha I, Oglesby E, Chow A, Kimball E, Pease ME, Schaub J, Quigley H. Rho-kinase inhibition reduces myofibroblast differentiation and proliferation of scleral fibroblasts induced by transforming growth factor beta and experimental glaucoma. *Trans Vis Sci Tech* 2018;**7**:6
14. Wettschureck N, Offermanns S. Rho/Rho-kinase mediated signaling in physiology and pathophysiology. *J Mol Med (Berl)* 2002;**80**:629–38
15. Dee RA, Mangum KD, Bai X, Mack CP, Taylor JM. Druggable targets in the Rho pathway and their promise for therapeutic control of blood pressure. *Pharmacol Ther* 2019;**193**:121–34
16. Fujita H, Fukumoto Y, Saji K, Sugimura K, Demachi J, Nawata J, Shimokawa H. Acute vasodilator effects of inhaled fasudil, a specific Rho-kinase inhibitor, in patients with pulmonary arterial hypertension. *Heart Vessels* 2010;**25**:144–9

17. Fukumoto Y, Yamada N, Matsubara H, Mizoguchi M, Uchino K, Yao A, Kihara Y, Kawano M, Watanabe H, Takeda Y, Adachi T, Osanai S, Tanabe N, Inoue T, Kubo A, Ota Y, Fukuda K, Nakano T, Shimokawa H. Double-blind, placebo-controlled clinical trial with a rho-kinase inhibitor in pulmonary arterial hypertension. *Circ J* 2013;**77**:2619–25
18. Ishikura K, Yamada N, Ito M, Ota S, Nakamura M, Isaka N, Nakano T. Beneficial acute effects of rho-kinase inhibitor in patients with pulmonary arterial hypertension. *Circ J* 2006;**70**:174–8
19. Li F, Xia W, Yuan S, Sun R. Acute inhibition of Rho-kinase attenuates pulmonary hypertension in patients with congenital heart disease. *Pediatr Cardiol* 2009;**30**:363–6
20. Zhou Q, Gensch C, Liao JK. Rho-associated coiled-coil-forming kinases (ROCKs): potential targets for the treatment of atherosclerosis and vascular disease. *Trends Pharmacol Sci* 2011;**32**:167–73
21. Meekins LC, Rosado-Adames N, Maddala R, Zhao JJ, Rao PV, Afshari NA. Corneal endothelial cell migration and proliferation enhanced by rho kinase (ROCK) inhibitors in in vitro and in vivo models. *Invest Ophthalmol Vis Sci* 2016;**57**:6731–8
22. Yi R, Xiao-Ping G, Hui L. Atorvastatin prevents angiotensin II-induced high permeability of human arterial endothelial cell monolayers via ROCK signaling pathway. *Biochem Biophys Res Commun* 2015;**459**:94–9
23. Jacobs M, Hayakawa K, Swenson L, Bellon S, Fleming M, Taslimi P, Doran J.The structure of dimeric ROCK I reveals the mechanism for ligand selectivity. *J Biol Chem* 2006;**281**:260–8
24. Jaffe AB, Hall A. Rho GTPases: biochemistry and biology. *Annu Rev Cell Dev Biol* 2005;**21**:247–69
25. Narumiya S, Thumkeo D. Rho signaling research: history, current status and future directions. *FEBS Lett* 2018;**592**:1763–76
26. Sawada N, Liao JK. Rho/Rho-associated coiled-coil forming kinase pathway as therapeutic targets for statins in atherosclerosis. *Antioxid Redox Signal* 2014;**20**:1251–67
27. Rana MK, Worthylake RA. Novel mechanism for negatively regulating Rho-kinase (ROCK) signaling through Coronin1B protein in neuregulin 1 (NRG-1)-induced tumor cell motility. *J Biol Chem* 2012;**287**:21836–45
28. Tu D, Li Y, Song HK, Toms AV, Gould CJ, Ficarro SB, Marto JA, Goode BL, Eck MJ. Crystal structure of a coiled-coil domain from human ROCK I. *PLoS One* 2011;**6**:e18080
29. Ueda K, Ohta Y, Hosoya H. The carboxy-terminal Pleckstrin homology domain of ROCK interacts with filamin-A. *Biochem Biophys Res Commun* 2003;**301**:886–90
30. Kubo T, Hata K, Yamaguchi A, Yamashita T. Rho-ROCK inhibitors as emerging strategies to promote nerve regeneration. *Curr Pharm Des* 2007;**13**:2493–9
31. Kubo T, Yamashita T. Rho-ROCK inhibitors for the treatment of CNS injury. *Recent Pat CNS Drug Discov* 2007;**2**:173–9
32. Maruta H, Nheu TV, He H, Hirokawa Y. Rho family-associated kinases PAK1 and rock. *Prog Cell Cycle Res* 2003;**5**:203–10
33. Miyamoto C, Maehata Y, Motohashi K, Ozawa S, Ikoma T, Hidaka K, Wada-Takahashi S, Takahashi SS, Yoshino F, Yoshida A, Kubota E, Hata R, Lee MC. Fasudil, a Rho kinase inhibitor, suppresses tumor growth by inducing CXCL14/BRAK in head and neck squamous cell carcinoma. *Biomed Res* 2014;**35**:381–8
34. Wang Y, Lu Y, Chai J, Sun M, Hu X, He W, Ge M, Xie C. Y-27632, a Rho-associated protein kinase inhibitor, inhibits systemic lupus erythematosus. *Biomed Pharmacother* 2017;**88**:359–66
35. Satoh S, Ikegaki I, Kawasaki K, Asano T, Shibuya M. Pleiotropic effects of the rho-kinase inhibitor fasudil after subarachnoid hemorrhage: a review of preclinical and clinical studies. *Curr Vasc Pharmacol* 2014;**12**:758–65
36. Narumiya S, Ishizaki T, Uehata M. Use and properties of ROCK-specific inhibitor Y-27632. *Meth Enzymol* 2000;**325**:273–84
37. Guan R, Xu X, Chen M, Hu H, Ge H, Wen S, Zhou S, Pi R. Advances in the studies of roles of Rho/Rho-kinase in diseases and the development of its inhibitors. *Eur J Med Chem* 2013;**70**:613–22
38. Steichen JM, Kuchinskas M, Keshwani MM, Yang J, Adams JA, Taylor SS. Structural basis for the regulation of protein kinase A by activation loop phosphorylation. *J Biol Chem* 2012;**287**:14672–80
39. Nakagawa O, Fujisawa K, Ishizaki T, Saito Y, Nakao K, Narumiya S. ROCK-I and ROCK-II, two isoforms of Rho-associated coiled-coil forming protein serine/threonine kinase in mice. *FEBS Lett* 1996;**392**:189–93
40. Ding H, Griesel C, Nimtz M, Conradt HS, Weich HA, Jager V. Molecular cloning, expression, purification, and characterization of soluble full-length, human interleukin-3 with a baculovirus-insect cell expression system. *Protein Expr Purif* 2003;**31**:34–41
41. White CR, Zehr JE. Spontaneous rhythmic contractile behaviour of aortic ring segments isolated from pressure loaded regions of the vasculature. *Cardiovasc Res* 1990;**24**:953–8
42. Williams ML, Kostrominova TY, Arruda EM, Larkin LM. Effect of implantation on engineered skeletal muscle constructs. *J Tissue Eng Regen Med* 2013;**7**:434–42
43. Colazet M, Chames P. Phage display and selections on purified antigens. *Methods Mol Biol* 2018;**1827**:165–78
44. He B, Dzisoo AM, Derda R, Huang J. Development and application of computational methods in phage display technology. *Curr Med Chem* 2018 2018/06/30. DOI: 10.2174/0929867325666180629123117.
45. van Nieuw Amerongen GP, Koolwijk P, Versteilen A, van Hinsbergh VW. Involvement of RhoA/Rho kinase signaling in VEGF-induced endothelial cell migration and angiogenesis in vitro. *Arterioscler Thromb Vasc Biol* 2003;**23**:211–7
46. Liu PY, Liao JK. A method for measuring Rho kinase activity in tissues and cells. *Meth Enzymol* 2008;**439**:181–9
47. Kimura K, Ito M, Amano M, Chihara K, Fukata Y, Nakafuku M, Yamamori B, Feng J, Nakano T, Okawa K, Iwamatsu A, Kaibuchi K. Regulation of myosin phosphatase by Rho and Rho-associated kinase (Rho-kinase). *Science* 1996;**273**:245–8
48. Kai H, Kuwahara F, Tokuda K, Imaizumi T. Diastolic dysfunction in hypertensive hearts: roles of perivascular inflammation and reactive myocardial fibrosis. *Hypertens Res* 2005;**28**:483–90
49. Yamamoto K, Masuyama T, Sakata Y, Nishikawa N, Mano T, Yoshida J, Miwa T, Sugawara M, Yamaguchi Y, Ookawara T, Suzuki K, Hori M. Myocardial stiffness is determined by ventricular fibrosis, but not by compensatory or excessive hypertrophy in hypertensive heart. *Cardiovasc Res* 2002;**55**:76–82
50. Fan D, Takawale A, Lee J, Kassiri Z. Cardiac fibroblasts, fibrosis and extracellular matrix remodeling in heart disease. *Fibrogenesis Tissue Repair* 2012;**5**:15
51. Baum J, Duffy HS. Fibroblasts and myofibroblasts: what are we talking about? *J Cardiovasc Pharmacol* 2011;**57**:376–9
52. Hattori T, Shimokawa H, Higashi M, Hiroki J, Mukai Y, Kaibuchi K, Takeshita A. Long-term inhibition of Rho-kinase suppresses left ventricular remodeling after myocardial infarction in mice. *Circulation* 2004;**109**:2234–9
53. Ohashi K, Nagata K, Maekawa M, Ishizaki T, Narumiya S, Mizuno K. Rho-associated kinase ROCK activates LIM-kinase 1 by phosphorylation at threonine 508 within the activation loop. *J Biol Chem* 2000;**275**:3577–82
54. Abreu-Blanco MT, Watts JJ, Verboon JM, Parkhurst SM. Cytoskeleton responses in wound repair. *Cell Mol Life Sci* 2012;**69**:2469–83
55. Do e Z, Fukumoto Y, Sugimura K, Miura Y, Tatebe S, Yamamoto S, Aoki T, Nochioka K, Nergui S, Yaoita N, Satoh K, Kondo M, Nakano M, Wakayama Y, Fukuda K, Nihei T, Kikuchi Y, Takahashi J, Shimokawa H. Rho-kinase activation in patients with heart failure. *Circ J* 2013;**77**:2542–50
56. Thenappan T, Shah SJ, Rich S, Tian L, Archer SL, Gomberg-Maitland M. Survival in pulmonary arterial hypertension: a reappraisal of the NIH risk stratification equation. *Eur Respir J* 2010;**35**:1079–87
57. Stevenson W, Cheng SF, Dastjerdi MH, Ferrari G, Dana R. Corneal neovascularization and the utility of topical VEGF inhibition: ranibizumab (Lucentis) vs bevacizumab (Avastin). *Ocul Surf* 2012;**10**:67–83
58. Thumkeo D, Watanabe S, Narumiya S. Physiological roles of Rho and Rho effectors in mammals. *Eur J Cell Biol* 2013;**92**:303–15

(Received March 4, 2019, Accepted April 11, 2019)